Title

Impact of initial effective stress on the thermo-mechanical behavior of normally consolidated clay

Authors

Samarakoon, Radhavi A
Kreitzer, Isaac L
McCartney, John S

Publication Date

2022-12-01

DOI

10.1016/j.gete.2022.100407

Peer reviewed

Impact of initial effective stress on the thermo-mechanical behavior of normally consolidated clay

Radhavi A. Samarakoon, Ph.D.

Post-doctoral Research Associate, Lawrence Berkeley National Laboratory, 1 Cyclotron Rd, Berkeley, CA 94720, USA; Email: rabeysir@eng.ucsd.edu

Isaac L. Kreitzer, B.S.

Graduate Research Assistant, Department of Structural Engineering, University of California San Diego, La Jolla, CA 92093-0085, USA; Email: ikreitzer@ucsd.edu

John S. McCartney, Ph.D., P.E., F.ASCE

Professor and Department Chair - Department of Structural Engineering, University of California San Diego, La Jolla, CA 92093-0085, USA. mccartney@ucsd.edu *(Corresponding Author)*

Abstract This study aims to investigate the impact of initial mean effective stress on the thermo-mechanical behavior of saturated normally consolidated kaolinite clay. Specifically, a series of isotropic thermal triaxial tests in a cell equipped with image analysis for volume change tracking was performed to understand the impact of the initial mean effective stress on the drained thermal volume change response as well as the undrained shear strength before and after drained heating. Anisotropically consolidated clay specimens were recompressed isotropically to four different initial mean effective stresses corresponding to normally consolidated conditions before drained heating and undrained shearing. While contractive volumetric strains were observed during drained heating of all normally consolidated specimens, the thermal radial strains were greater than thermal axial strains due to the application of isotropic stresses after anisotropic consolidation from a slurry. The magnitude of thermal volumetric strain increased with increasing initial mean effective stress, which is a departure from expected trends from established constitutive models. A corresponding increase in undrained shear strength with both temperature and initial mean effective stress was observed. The results indicate the need for considering the impact of initial mean effective stress in geotechnical applications involving normally consolidated clay under non-isothermal conditions.

Keywords: Thermo-mechanical behavior, volume change, undrained shear strength, clay

1. Introduction

The thermo-mechanical behavior of clay has become an important topic of research because of increased interest in geomechanical problems involving thermal effects. As most of these geomechanical problems studied in the literature involved overconsolidated or compacted clays (i.e., cast-in-place energy piles, buffer systems for nuclear waste repositories, backfill for buried electrical cables), there has not been a significant amount of attention on investigating the thermo-mechanical behavior of soft, normally consolidated clays. Recently, there has been interest in using in-situ heating to improve the engineering properties of soft clay (Abuel-Naga et al. 2006; Pothiraksanon et al. 2010; Samarakoon and McCartney 2020a, 2021; Ghaaowd and McCartney 2021; Ghaaowd et al. 2022). In-situ thermal soil improvement combines geothermal heat exchangers with vertical drains, which will be embedded in a soft clay deposit transferring heat to the surrounding soil. In addition to being used during the preconsolidation stage to expedite consolidation, the ground heat exchangers can also be used as an underground heat storage system for the building after soil improvement has been completed. When assessing thermal soil improvement methods, it is important to understand the thermo-mechanical behavior of soft clays at different initial mean effective stresses indicative of different depths in a clay layer. Within the domain of soil improvement, this study aims to investigate the role of initial effective stress on the thermo-mechanical behavior of normally consolidated clay subjected to drained heating. Specifically, the effect on undrained shear strength and volume change is considered.

Several researchers have investigated the thermo-mechanical response of clay (Campanella and Mitchell 1968; Hueckel and Baldi 1990; Cekerevac and Laloui 2004; Abuel-Naga et al. 2007a). Undrained heating of saturated clays leads to an increase in excess pore water pressure whereas drained heating of saturated clays results in thermal volume changes depending on the stress history of the clay. The thermal volume change of highly overconsolidated clays was observed to be expansive, elastic, and recoverable, whereas the thermal volume change of normally consolidated clays was contractive, plastic, and partly irrecoverable. Although thermal volumetric strains are much smaller in comparison to volumetric strains obtained by mechanical loading, the reduction in void ratio obtained during drained heating leads to an increase in undrained shear strength for normally consolidated clays (Houston et al. 1985). The undrained shear strength of clay was observed to be dependent on temperature and different trends were seen based on the drainage conditions during heating (Houston et al. 1985; Kuntiwattanakul et al. 1995; Tanaka 1997; Abuel-Naga 2006). In general, normally consolidated clay specimens subjected to shear after undrained heating showed a decrease in undrained shear strength with temperature whereas specimens subjected to drained heating resulted in an increase in undrained shear strength with increasing temperature.

Constitutive models describing the thermo-mechanical behavior of clays have been developed by several researchers (Hueckel and Borsetto 1990; Cui et al. 2000; Laloui and Cekerevac 2003; Abuel-Naga et al. 2007a; Abuel-Naga et al. 2009). The thermal volume changes in these models are typically driven by changes in the apparent preconsolidation or yield stress with temperatures. As an artifact of this approach to predict thermal volume changes, these models predict the same amount of thermal volume change for normally consolidated clays, irrespective of the initial stress state or void ratio. The constitutive models were generally validated using tests conducted on initially overconsolidated clay specimens which were mechanical loaded to a normally consolidated state after drained heating to different elevated temperatures to define a relationship between the yield stress and temperature. Compression curves obtained from isothermal tests carried out at elevated temperatures showed compression curves with slopes similar to that of a compression curve at room temperature but with a shift to the left. The constitutive models developed based on these observations predicted that normally consolidated clays will have the same thermal hardening response and the same amount of volume change regardless of its initial mean effective stress. While many of the models included successful validation of the volume change of a single normally consolidated clay specimen, they did not validate the model for several normally consolidated clay specimens with different initial stresses.

On the other hand, field tests (Bergenstahl et al. 1994), laboratory tests (Abuel-Naga et al. 2007b; Uchaipichat and Khalili 2009; Ghaaowd et al. 2017) and poromechanics theories (Campanella and Mitchell 1968) show that normally consolidated, saturated clay having different initial mean effectives stresses and void ratios lead to different thermal pressurization effects during undrained heating. The effect of the initial effective stress state on the thermal pressurization process leads to the hypothesis that the thermal volume change of normally consolidated clays will also be dependent on the initial mean effective stress for normally consolidated clays. However, there are limited studies in the literature where the thermal behavior of normally consolidated clays at different initial mean effective stress states were carefully investigated. In previous studies conducted by the authors on normally consolidated kaolinite specimens, it was observed that the thermal volume change and undrained shear strength was dependent on the initial mean effective stress (Samarakoon et al. 2018; Samarakoon and McCartney 2020b). Based on the observations of excess pore water pressure behavior under undrained conditions and limited experimental data on thermal volume change of normally consolidated clays, there is a need to further investigate the effect of initial mean effective stress on the thermo-mechanical behavior of normally consolidated clays. To that end, this study presents the results from an experimental investigation involving drained heating of saturated normally consolidated kaolinite specimens at different initial mean effectives stresses representative of different depths in a clay deposit.

2. Material and Methods

2.1 Material

Commercial kaolinite clay obtained from M&M Clays Inc. of McIntyre, GA was used in this study. The properties of the Georgia kaolinite clay are summarized in Table 1, including the compression indices obtained from an isotropic compression test at room temperature. The Georgia kaolinite clay is classified as CL according to the Unified Soil Classification System (USCS).

2.2 Experimental set-up

The laboratory tests were conducted using a modified triaxial system developed by Alsherif and McCartney (2015). A schematic of the experimental set-up is shown in Fig. 1. The triaxial system comprised of a Pyrex cell capable of withstanding high temperatures and pressures applied during testing. Heat was applied to the cell by circulating heated water from a temperature-controlled circulating bath through a stainless-steel U-shaped pipe placed inside the cell. A circulation pump able to accommodate high temperatures and pressures was used to ensure uniform mixing of cell water. Two thermocouples were placed to measure the temperature of the cell fluid and at the bottom of the specimen respectively. The thermocouple at the bottom of the specimen was included as it was presumed that greater heat losses would occur through the base pedestal of the specimen, potentially leading to lower temperatures in this region of the specimen. The temperature recorders were accurate to 0.5 °C. The cell pressure was applied using a flow pump whereas the back-pressure was controlled using a pressure panel.

Drainage was allowed only from the top of the specimen. Changes in the pore water pressure were monitored at the bottom of the specimen using a pore water pressure transducer.

Obtaining volume change measurements using outflow pipettes is challenging at elevated temperatures due to the thermal expansion of the system. Therefore, the volume change was measured using an image analysis technique in a non-contact manner. Two high resolution cameras (Nikon D7500) were used to capture the images of the specimen at specified time intervals throughout the duration of the test. For a given time, images were captured from two planes of the specimen which are perpendicular to each other. Images were converted to a binary form and the total volume of the specimen was obtained from the summation of discrete volumes associated with a series of stacked disks where the height of a single disk (Δh) was one vertical pixel, and the diameter (d) was the number of horizontal pixels (Uchaipichat et al. 2011). 2D to 3D mapping for a single disk is shown in Eq. (1) and the total volume of the specimen is obtained as shown in Eq. (2) where n is the number of vertical pixels for Δh = 1 pixel.

$$Volume\ of\ a\ single\ disk = \pi d^2 \Delta h/4 \quad (1)$$

$$Total\ volume\ of\ specimen = \sum_{i=1}^{n} \pi {d_i}^2 \Delta h_i/4 \quad (2)$$

An average of the volumes calculated from the two image planes was taken as the total volume of the specimen at a given time. Examples of images from the stages of processing and typical results during different stages of triaxial testing are shown in Fig. 2. Void ratios obtained from image analysis during consolidation are shown in Fig. 3, along with a comparison of void ratios obtained from pipette readings. Good agreement is seen in the trends of void ratio changes during consolidation between the measurements obtained from image analysis and pipette readings. In addition to directly calculating changes in volume using Equation (2), the results from these image analyses can be used to interpret the axial and radial thermal strains, which may be useful in interpreting the thermal volume change response.

2.3 Procedure

The clay specimens were prepared by forming a slurry from clay and deionized water at a gravimetric water content of 130% in a commercial planetary mixer. The slurry was then poured into a hollow steel cylinder of diameter 88.9 mm with porous stones and filter paper placed on both top and bottom. The slurry was first consolidated anisotropically using a compression frame at a constant rate of 0.04 mm/min for 48 hours. Then constant vertical stresses of 26, 52, 103 and 181 kPa were applied in 24 hour-long increments. At the end of this process, the clay layer was extruded from the steel cylinder and trimmed into a cylindrical specimen with a diameter of 72.4 mm and height of 145 mm, making it suitable for testing in the thermal triaxial cell. The specimen was back-pressure saturated by applying cell pressure and back-pressure in stages until the Skempton's pore water pressure parameter B was at least 0.95. Then the specimen was isotropically consolidated by applying a specified mean effective stress. Four different mean effective stresses were considered in this study as 230, 260, 290 and 320 kPa respectively. While these mean effective stresses are on the high range for the thermal soil improvement application discussed above, these values were chosen to ensure that the specimens were at normally consolidated conditions at the stress states considered. It is assumed that normally consolidated clay specimens at lower mean effective stresses will also have the same behavior as past studies have shown that stress history is the most important variable in the thermo-mechanical behavior of clays (e.g., Hueckel and Borsetto 1990; Cui et al. 2000; Laloui and Cekerevac 2003; Abuel-Naga et al. 2007a; Abuel-Naga et al. 2009).

A total of 8 tests were conducted in this study, with each test requiring approximately 2 weeks to perform including specimen preparation. The first set of tests were at room temperature (24 °C), where 4 specimens were first isotropically consolidated to the 4 different mean effective stresses mentioned above respectively. In these tests the cell pressure was increased using ramp loading and the back pressure was maintained constant to subject the specimen to the specified effective stress. The applied isotropic stress state was maintained until the volume change of the specimen reached steady state. After reaching the end of primary consolidation, the specimens were sheared under undrained conditions. The second set of tests were conducted at the same mean effective stresses mentioned above but under elevated temperature. Specifically, after reaching the end of primary consolidation under the target mean effective stresses in the thermal triaxial cell, the specimens were subjected to drained heating where the cell temperature was increased from room temperature to 59.5 °C. After the specimens reached thermo-mechanical equilibrium, they were subjected to undrained shearing at the elevated temperature. A summary of the thermo-mechanical stress paths for the thermal triaxial tests are shown in Fig. 4.

3. Results

3.1 Typical Time Series Results

The change in mean effective stress, excess pore water pressure and temperature for a typical thermal triaxial test (target mean effective stress at heating = 290 kPa) is shown in Fig. 5. The mean effective stress increases during isotropic consolidation and remains constant throughout the test apart from a slight decrease observed at the onset of heating. Correspondingly, an increase in pore water pressure is also observed at the onset of heating. This is due to the relatively fast rate of increase in temperature at the beginning of the heating stage. With the sudden increase in temperature and the low permeability of the clay specimen, partially drained conditions prevail at the beginning of the heating stage. As the temperature stabilizes with time and the excess pore water pressures dissipate, the mean effective stress returns to its original value. The temperature is measured at the top of the cell as well as the bottom of the specimen. Although both measurements of temperature follow similar trends, a difference of 8.6 °C is observed between the two locations during heating. This is a relatively large difference that is likely due to greater thermal losses through the base pedestal of the cell. Nonetheless, all heated tests were performed with the same conditions, so the effects of the mean effective stress could still be assessed. The cell temperature is shown in all subsequent figures as it is assumed to represent the temperatures on the top and sides of the cylindrical specimen.

An advantage of using the image analysis for strain measurement is that the axial and radial strains can be calculated separately in addition to the volumetric strain. As mentioned, the specimen was divided into a series of stacked disks where the height of a disk was one pixel. The diameter at a given height was the number of horizontal pixels. The diameter of the specimen at a given time was obtained using an average of diameter values obtained along the height of the specimen. The height of the specimen was obtained in a similar manner where it was discretized into vertical disks. The variations in axial and radial strains during isotropic consolidation and drained heating are shown in Fig. 6(a) for a typical thermal triaxial test performed at a target initial mean effective stress of 290 kPa. In this test, the radial strain measured during isotropic consolidation is greater than the axial strain. Furthermore, the rate of increase in strain at the beginning of consolidation is higher in the radial direction. During drained heating, the thermal strains show a similar behavior where more deformation is observed in the radial direction with a smaller increase in axial strain. The radial strain can be observed to be compressive during heating followed by a slight expansion. The variation of axial and radial strains during drained heating is shown in Fig. 6(b). Similar behavior was observed for the specimens at other initial mean effective stresses.

The reason for the difference in axial and radial strains during heating under an isotropic stress state is likely due to the preparation of the clay specimens using anisotropic consolidation from a slurry. The kaolinite slurry was consolidated in a cylindrical mold in an oedometric stress state. The slurry was first consolidated by applying a constant strain rate and then subjected to vertical stress incrementally. As no strain was allowed in the radial direction, K_0 conditions can be assumed during the specimen preparation stage. During triaxial testing however, the specimens were consolidated to a normally consolidated state under an isotropic stress state. As a result of the specimen preparation process under K_0 conditions, the behavior of the specimen may be affected by stress-induced anisotropy. Most studies evaluating thermal volume change behavior were conducted using oedometers or triaxial cells and the results are typically reported as volumetric strains. However, the presence of stress-induced anisotropy may impact the deformation of the specimen when subjected to mechanical and thermal loading. Coccia and McCartney (2012) developed a new thermo-hydro-mechanical true triaxial cell which had the ability to subject soil specimens to different anisotropic stress states. Tests were conducted on cubical specimens of saturated overconsolidated Bonny silt and plastic contraction in the major stress direction and elastic expansion in the minor stress direction was observed as the initial stress anisotropy increased during heating. Similar observations were made by Shanina and McCartney (2017) for cubical specimens of unsaturated silt. To assess this, radial and axial strain trends during isotropic consolidation and drained heating were investigated. While the reason for reporting thermal deformations in the literature only in terms of void ratio or volumetric strain may be the difficulty of measuring both axial and radial strains in conventional triaxial and oedometric tests. This issue was resolved in this study using image analysis for measurement of axial and radial strains.

Based on these observations, although the specimens were subjected to isotropic stress states in the thermal triaxial cell, the strain response of the specimens during mechanical loading and heating was anisotropic with greater radial strains than axial strains. This may be due to the specimen preparation process where the specimen was consolidated under axial loading in the vertical direction with no allowance for radial deformation. As the specimen continued to contract during drained heating, similar behavior is observed. Although the thermal strains are smaller in comparison, radial strain during drained heating is still observed to be larger than the axial strain. Hueckel and Pellegrini (1996) obtained similar results for Boom clay where plastic contractive strain was larger in the horizontal direction than in the vertical direction during heating under an isotropic stress state. The component of horizontal stress during isotropic loading is higher than that during K_0 consolidation. It was speculated that the arrangement of clay microstructure during K_0 compression may mainly leave space between horizontal neighboring clusters and their closure during heating will results in larger lateral thermal strains. Hattab and Fleureau (2011) experimentally investigated the orientation of kaolinite microstructure during different stages of loading using SEM picture analysis. Similar to this study, specimens were first anisotropically consolidated and a structural anisotropy with a preferred orientation of particles in the horizontal direction was observed from the SEM images. After subsequent isotropic compression in a triaxial cell, a rotation of particles and a decrease in pore space was observed reflecting a tendency towards structural isotropy.

The variations in void ratio and temperature are shown in Fig. 6(c) for a typical test at a target initial mean effective stress of 290 kPa during mechanical consolidation and drained heating. As expected, the void ratio decreases during mechanical consolidation and a further decrease is observed during drained heating. In comparison, the change in void ratio during drained heating for a cell temperature increase of 35.5 °C is smaller than that obtained during mechanical consolidation. Care was taken to ensure that primary consolidation was completed prior to starting the heating stage. The variation in void ratio during drained heating is shown in Fig. 6(d). Similar to the radial strain, the void ratio decreases indicating compression during heating, followed by a slight expansion. The compression curve for the same test is shown in Fig. 7. During drained heating, the specimen is subjected to contractive volume change at the given target mean effective stress.

3.2 Consolidated Undrained Shearing Results

For the heated tests, once the specimens reached equilibrium during the drained heating stage, they were subjected to shear under undrained conditions. The specimens tested at room temperature were sheared under undrained conditions after primary consolidation was completed. The consolidated undrained triaxial compression test results for specimens at room temperature and after heating are shown in Fig. 8. The principal stress ratio versus axial strain, maximum principal stress difference versus axial strain and excess pore water pressure versus axial strain are shown in Figs. 8(a), 8(b), and 8(c), respectively. In the tests on heated and not heated tests, the principal stress ratios in Fig. 8(a) increase nonlinearly until reaching a peak value at an axial strain of approximately 15%, at which point the maximum frictional response of the specimens is mobilized. The maximum principal stress differences in Fig. 8(b) increased nonlinearly to a maximum value at axial strains between 10 and 15%, followed by a slight softening with continued shearing. The excess pore water pressure in Fig. 8(c) was positive in all tests and increased until reaching a maximum value at axial strains ranging from 10-15%. In comparison to the tests on specimens at room temperature, an increase in the maximum principal stress difference is observed for the specimens sheared at a cell temperature of 59.5 °C for all initial mean effective stresses considered. The excess pore water pressure generated during shear was smaller at 59.5 °C for the initial mean effective stresses considered, which led to a greater mean effective stress at failure for the heated specimens. Overall, the stress-strain curves in Figure 8 correspond to those expected for normally consolidated clays for the unheated specimens and to those expected for lightly overconsolidated clays for the heated specimens.

The effective stress paths for the normally consolidated specimens sheared at room temperature and after heating are shown in Fig. 9(a). The maximum principal stress difference values fall onto the same peak failure envelope irrespective of their heating path. A similar observation was made in a previous study conducted by the authors where different heating paths at different initial mean effective stresses were considered (Samarakoon et al. 2018). The stress paths during consolidated undrained shearing at 24 °C are correspond to those expected for normally consolidated clays. On the other hand, for the mean effective stress states of 230, 260 and 290 kPa, the stress paths correspond to a lightly overconsolidated state. This behavior is consistent with the results observed in literature where an overconsolidated behavior was observed in initially normally consolidated specimens upon further mechanical loading after drained heating (Towhata et al. 1993; Sultan et al. 2002). It also conforms to the thermal hardening phenomena experienced by the soil subjected to an increase in temperature. The relationship between the maximum principal stress difference and the mean effective stress at failure for the 8 clay specimens is shown in Fig. 9(b). The markers represent the peaks of the maximum principal stress difference and the corresponding mean effective stress at failure, so the slope of the best fit line corresponds to the slope of the peak failure envelope. However, this line can be assumed to coincide with the critical state line for this clay as it coincides with the point of stress path tangency observed in the effective stress paths in Fig. 9(a).

4. Analysis

4.1 Thermal volume change

A comparison of the thermal strains at different initial mean effective stresses is shown in Fig. 10. The thermal volumetric strains obtained after drained heating at different initial mean effective stresses shown in Fig. 10(a) were compressive with a positive sign. The thermal volumetric strains range from 0.40% - 0.94% which are consistent with volumetric strain values reported in the literature for normally consolidated clays during drained heating for this temperature change (Hueckel and Baldi, 1990; Baldi et al. 1988; Delage et al. 2004; Cekerevac and Laloui 2004). The contractive volumetric strains after heating increased with increasing initial mean effective stress. This observation confirms that thermal volume change of normally consolidated clay is dependent on the initial mean effective stress, as hypothesized. It is also in accordance with the increasing trends in excess pore water generation with increasing initial mean effective stress reported by Abuel-Naga et al. (2007b) and Ghaaowd et al. (2017). The authors made similar observations in kaolinite specimens subjected to a drained heating cooling cycle in a previous study (Samarakoon and McCartney 2020b). During drained heating, the thermal volumetric strain was observed to increase as the initial mean effective stress increased, which is also shown in Fig. 10(b). The results shown in Fig. 10(b) also indicate that the thermal axial strain and thermal radial strain increase slightly with the initial mean effective stress, with a greater increase in thermal axial strain than thermal radial strain with increasing initial mean effective stress. It should be noted that the radial and axial strains were calculated based on an average diameter and height of the specimen as described in Section 3.1 whereas the volumetric strains were obtained by considering the summations of volumes associated with a series of stacked disks. The ratios between axial strain and radial strain for normally consolidated specimens at different initial mean effective stresses is shown in Fig. 10(c). The ratios are less than 1 because the radial strain was greater than the axial strain. As expected, the strain observed during isotropic consolidation is higher than the strain during drained heating. An interesting observation is that the ratio between axial strain and radial strain increases with increasing initial mean effective stress. This indicates that as the initial mean effective stress increases, the strain response of the specimen is less anisotropic. The anisotropic strain response observed during drained heating may not be a result of thermal behavior of the clay but rather due to the inherent anisotropy in the specimen caused by the anisotropic consolidation process during specimen preparation. Although the specimen is mechanically loaded to a normally consolidated state prior to heating, there may still exist some degree of anisotropy in the specimen. As a result, we may continue to observe an anisotropic strain response as the specimen is subjected to thermal loading. Based on observations by both Coccia and McCartney (2012) and Shanina and McCartney (2017) the inherent anisotropy from soil preparation (static compaction in their case) did not have a significant impact on the overall thermal volumetric strains but only on the strain response in different directions. The results in Fig. 10(c) indicate that the impact of the specimen anisotropy is less significant as the initial mean effective stress increases. Although the stress-induced anisotropy in the test specimens considered in this study was a result of the preparation process, the anisotropic stress state is representative of natural soil deposits in at rest conditions. Characterizing the thermal deformation of clays with inherent anisotropy can be useful in geotechnical applications involving thermal effects.

4.2 Undrained shear strength

Undrained shear strength values obtained for the normally consolidated specimens tested at different initial mean effective stresses are summarized in Fig. 11. Results for the specimens sheared at both room temperature as well as 59.5 °C are shown. It is assumed that the maximum principal stress difference corresponds to the undrained shear strength of the soil. A clear increase in undrained shear strength can be seen for the specimens sheared after heating. This increase in undrained shear strength can be attributed to the plastic volumetric contraction which occurred during drained heating. Like the results obtained for thermal volume change, the increase in undrained shear strength after heating is observed to increase with increasing initial mean effective stress. As described in the previous section, a higher degree of thermal volume change was observed as the initial mean effective stress increased. As a result of this plastic decrease in volume, the undrained shear strength after heating is also observed to increase with increasing initial mean effective stress.

These results are in contrast with a previous observation made by the authors (Samarakoon et al. 2018) where the amount of increase in undrained shear strength after drained heating was smaller for specimens with greater initial mean effective stresses. However, this observation from the previous study was counterintuitive as it is expected that greater thermally induced excess pore water pressures are expected for clay with greater initial mean effective stresses (Ghaaowd et al. 2017). The authors attribute these inconsistencies to the differences in specimen preparation and the experimental procedures followed. For instance, the clay specimens in Samarakoon et al. (2018) were consolidated in a larger diameter mold during specimen preparation and quartered after extrusion to obtain four separate triaxial test specimens. In the current study, each triaxial specimen was consolidated individually in a smaller-diameter steel cylinder.

The results for thermal volumetric strain and the increase in undrained shear strength at different initial mean effective stresses are synthesized in Fig. 12. For the stress range considered in this study, the thermal volumetric strain and the undrained shear strength of normally consolidated kaolinite specimens is dependent on the initial mean effective stress. Based on the trends observed, the thermal volumetric strain and the corresponding increase in undrained shear strength increases with increasing initial mean effective stress. This is contrary to the existing thermo-elasto-plastic models where the same magnitude of volumetric strain is predicted for normally consolidated clays subjected to an increase in temperature irrespective of its initial mean effective stress. However, in applications involving normally consolidated clays such as improvement of soft clay deposits using in-situ heating, it is important to account for the effect of initial mean effective stress on the thermal behavior of clay. The findings from this study will enable users to strategically apply thermal soil improvement over different depths of a clay layer thus increasing the efficiency of the thermal soil improvement process.

5. Conclusion

This paper presents the results of an experimental study investigating the impact of initial mean effective stress on the thermo-mechanical behavior of saturated normally consolidated clay. Contrary to the existing thermo-elasto-plastic models, the thermal volumetric strain was observed to be dependent on the initial mean effective stress of the specimen. Thermal volumetric strain during drained heating was contractive and increased as the initial mean effective stress increased. Correspondingly, the undrained shear strength also increased with increasing initial mean effective stress. These findings are useful when configuring geothermal heat exchangers for soil improvement via in-situ heating where thermal soil improvement can be strategically applied over different depths of a clay layer. The specimen preparation process of anisotropic consolidation from a slurry was found to affect the strain response of the clay specimen where more deformation was observed in the radial direction during isotropic consolidation as well as drained heating. Further studies can be conducted on a broader range of soil types and stress states to better understand the trends of thermal behavior of normally consolidated clay and to incorporate the effect of initial mean effective stress into thermo-elasto-plastic constitutive models.

CRediT authorship contribution statement

Radhavi Samarakoon: Conceptualization, methodology, investigation, formal analysis, visualization, writing – original draft. **Isaac Kreitzer:** Investigation. **John McCartney:** Supervision, resources, funding acquisition, project administration, conceptualization, methodology, writing – review and editing.

Declaration of competing interest

The authors declare that they have no known competing financial interests or personal relationships that could have appeared to influence the work reported in this paper.

Acknowledgements

Funding from NSF grant CMMI 1941571 is appreciated. The opinions are those of the authors.

References

Abuel-Naga, H.M., Bergado, D.T., Chaiprakaikeow, S. (2006) "Innovative thermal technique for enhancing the performance of prefabricated vertical drain during the preloading process." *Geotextiles and Geomembranes*. 24, 359-370.

Abuel-Naga, H.M., Bergado, D.T., Bouazza, A., Ramana, G.V. (2007a) "Volume change behaviour of saturated clays under drained heating conditions: experimental results and constitutive modeling." *Canadian Geotechnical Journal*. 44, 942-956.

Abuel-Naga, H.M., Bergado, D.T., Bouazza, A. (2007b) "Thermally induced volume change and excess pore water pressure of soft Bangkok clay." *Engineering Geology*. 89, 144-154.

Abuel-Naga, H.M., Bergado, D.T., Bouazza, A., Pender, M. (2009) "Thermomechanical model for saturated clays." *Géotechnique*. 59(3), 273-278.

Alsherif, N. A., McCartney, J. S. (2015). "Nonisothermal behavior of compacted silt at low degrees of saturation." *Géotechnique*. 65(9), 703-716. DOI: 10.1680/geot./14 P 049.

Baldi, G., Hueckel, T., Pellegrini, R. (1988). "Thermal volume changes of the mineral-water system in low-porosity clay soils." *Canadian Geotechnical Journal*. 25, 807-825.

Bergenstahl, L., Gabrielsson, A., Mulabdic, M. (1994), "Changes in soft clay caused by increase in temperature." *Proc. 13th International Conference on Soil Mechanics and Foundation Engineering*. New Delhi, India. Jan 5-10. 1637-1641.

Campanella, R.G., Mitchell, J.K. (1968) "Influence of temperature variations on soil behavior." *Journal of the Soil Mechanics and Foundation Division. ASCE*. 94(3), 709-734.

Cekerevac, C., Laloui, L. (2004) "Experimental study of thermal effects on the mechanical behaviour of a clay." *International Journal for Numerical and Analytical Methods in Geomechanics*. 28, 209-228.

Coccia, C.J.R., McCartney, J.S. (2012) "A thermo-hydro-mechanical true triaxial cell for evaluation of the impact of anisotropy on thermally-induced volume changes in soils." *ASTM Geotechnical Testing Journal*. 35(2), 227-237.

Cui, Y. J., Sultan, N., Delage, P. (2000). "A thermomechanical model for clays." *Canadian Geotechnical Journal* 37(3), 607–620.

Delage, P., Cui, Y.J., Sultan, N. (2004). "On the thermal behaviour of Boom clay." *Proceedings of the Eurosafe Conference.* Berlin, Germany. 1–8.

Ghaaowd, I., Takai, A., Katsumi, T., McCarntey, J.S. (2017) "Pore water pressure prediction for undrained heating of soils." *Environmental Geotechnics*. 4(2), 70-78.

Ghaaowd, I., McCartney, J.S. (2021). "Centrifuge modeling methodology for energy pile pullout from saturated soft clay." *ASTM Geotechnical Testing Journal*. 45(2), 332-354.

Ghaaowd, I., McCartney, J.S., Saboya, Jr., F. (2022). "Centrifuge modeling of temperature effects on the pullout capacity of torpedo piles in soft clay." *Soils and Rocks. Special Issue on Energy Piles*. 45(1), e2022000822.

Hattab, M., Fleureau, J-M. (2011). "Experimental analysis of kaolinite particle orientation during triaxial path." *International Journal for Numerical and Analytical Methods in Geomechanics*. 35(8), 947-968.

Houston, S.L., Houston, W.N., Williams, N.D. (1985). "Thermo-mechanical behavior of seafloor sediments." *Journal of Geotechnical Engineering. ASCE*. 111(12), 1249-1263.

Hueckel, T., Baldi, M. (1990). "Thermoplasticity of saturated clays: Experimental constitutive study." *Journal of Geotechnical Engineering*. 116(12), 1778-1796.

Hueckel, T., Borsetto, M. (1990). "Thermoplasticity of saturated soils and shales: constitutive equations." *Journal of Geotechnical Engineering*. 116(12), 1765–1777.

Hueckel, T., Pellegrini, R. (1996). "A note on thermomechanical anisotropy of clays." *Engineering Geology*. 41, 171–180.

Kuntiwattanakul, P., Towhata, I., Ohishi, K., Seko, I. (1995). "Temperature effects on undrained shear characteristics of clay." *Soils and Foundation*. 35(1), 147-162.

Laloui, L., Cekerevac, C. (2003). "Thermo-plasticity of clays: an isotropic yield mechanism." *Computers and Geotechnics*. 30(8), 649–660.

Pothiraksanon, C., Bergado, D.T., Abuel-Naga, H.M. (2010) "Full-scale embankment consolidation test using prefabricated vertical thermal drains." *Soils and Foundations*. 50(5), 599-608.

Samarakoon, R.A., Ghaaowd, I., McCartney, J. S. (2018). "Impact of drained heating and cooling on undrained shear strength of normally consolidated clay." *Proc. 2nd International Symposium on Energy Geotechnics*. Lausanne. A. Ferrari, L. Laloui, eds., Vienna. 243-249.

Samarakoon, R.A., McCartney, J.S. (2020a). "Analysis of thermal drains in soft clay." *Proc. GeoAmericas 2020: 4th PanAm Conference on Geosynthetics*. Rio de Janeiro, Brazil. Oct 26-31. 1-9.

Samarakoon, R.A., McCartney, J.S. (2020b). "Role of initial effective stress on the thermal consolidation of normally consolidated clays." *Proc. 2nd International Conference on Energy Geotechnics (ICEGT-2020)*. E3S Web of Conferences, Les Ulis, France. 205, 09001.

Samarakoon, R.A., McCartney, J.S. (2021). "Performance of prefabricated thermal drains in soft clay." *Geosynthetics Conference 2021*. Kansas City, MO, USA. Feb 21-24. Nicks, J. and Beauregard, M., eds. IFAI, Roseville, MI. 1-12.

Shanina, M., McCartney, J.S. (2017). "Influence of anisotropic stress states on the thermal volume change of unsaturated silt." *Soils and Foundations*. 57(2), 252-266.

Sultan, N., Delage, P., Cui, Y.J. (2002). "Temperature effects on the volume change behavior of boom clay." *Engineering Geology*. 64, 135-145.

Tanaka, N., Graham, J. Crilly, T. (1997). "Engineering behaviour of reconstituted Illitic clay at different temperatures." *Engineering Geology*. 47(4), 339-350.

Towhata, I., Kuntiwattanakul, P., Seko, I., Ohishi, K. (1993). "Volume change of clays induced by heating as observed in consolidation tests." *Soils and Foundations*. 33(4), 170-183.

Uchaipichat, A., Khalili, N. (2009). "Experimental investigation of thermo-hydro-mechanical behaviour of an unsaturated silt." *Géotechnique*. 59(4), 339–353.

Uchaipichat, A., Khalili, N., Zargarbashi, S. (2011). "A temperature controlled triaxial apparatus for testing unsaturated soils." *Geotechnical Testing Journal*. 34(5), 1-9.

Table 1 Properties of Georgia kaolinite clay

Parameter	Value
Liquid Limit	47
Plasticity Index	19
Specific Gravity	2.6
Slope of VCL (λ)	0.09
Slope of RCL (κ)	0.02
USCS Classification	CL

List of Figure Captions (Figures to use color in print: 2, 5, 6, 7, 8, 9, 10)

Fig. 1. Schematic of the thermal triaxial setup

Fig. 2. Image processing: (a) Examples of images from the three stages of processing; (b) Typical results from processed images for different stages of triaxial testing

Fig. 3. Typical void ratio measurements: (a) Void ratio variations measured using image analysis during consolidation; (b) Comparison of void ratios measured using images analysis and outflow pipette readings

Fig. 4. Summary of the thermo-mechanical paths for the triaxial testing program

Fig. 5. Changes in mean effective stress and temperature for a typical thermal triaxial test (target mean effective stress at heating = 290 kPa)

Fig. 6. Thermo-mechanical volume changes during different stages of a typical thermal triaxial test at a target mean effective stress at heating = 290 kPa(Vertical gray dashed line denotes the time when isotropic mechanical consolidation is complete and drained heating commences): (a) Variation in axial and radial strains; (b) Variation in axial and radial strains during drained heating; (c) Variation in void ratio; (d) Variation in void ratio during drained heating

Fig. 7. Compression curve during thermo-mechanical loading from a typical thermal triaxial test (target mean effective stress at heating = 290 kPa)

Fig. 8. Consolidated Undrained (CU) triaxial compression test results for unheated and heated normally consolidated kaolinite: (a) Principal stress ratio vs. axial strain (b) Maximum principal stress difference vs. axial strain (c) Excess pore water pressure vs. axial strain

Fig. 9. (a) Effective stress paths for unheated and heated normally consolidated kaolinite; (b) Relationship between maximum principal stress difference and mean effective stress at failure for normally consolidated kaolinite specimens sheared at room temperature and after heating

Fig. 10. (a) Thermal volumetric strains for normally consolidated kaolinite at different initial mean effective stresses as a function of temperature; (b) Thermal strains for normally consolidated kaolinite as a function of initial mean effective stress; (c) Axial to radial strain ratios for normally consolidated kaolinite specimens at different initial mean effective stresses

Fig. 11. Undrained shear strength values for unheated and heated normally consolidated kaolinite at different initial mean effective stresses

Fig. 12. Summary of thermal volumetric strain and increase in undrained shear strength after heating of normally consolidated kaolinite at different initial mean effective stresses

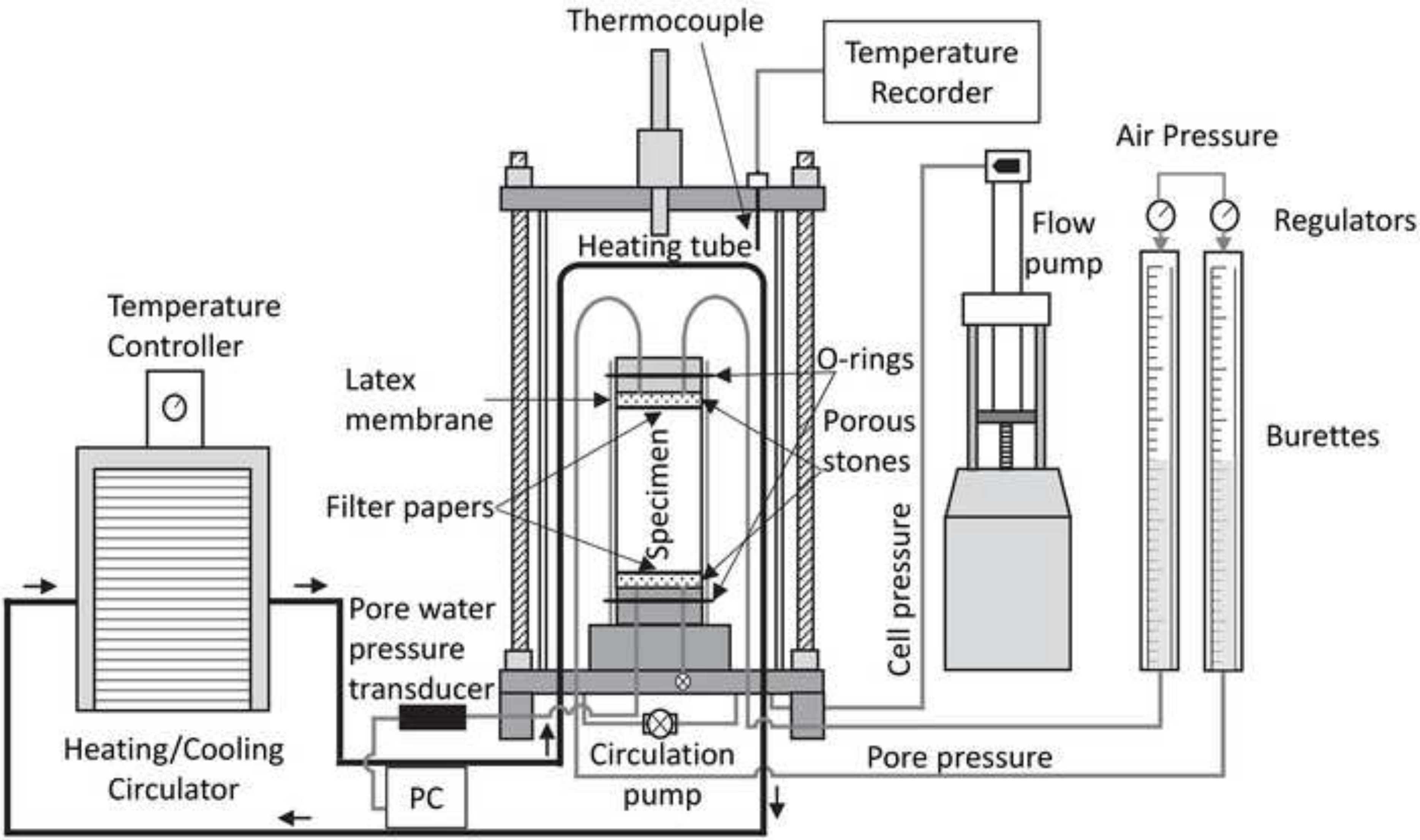
Thermocouple
Temperature Recorder
Air Pressure
Flow pump
Regulators
Heating tube
Temperature Controller
O-rings
Latex membrane
Porous stones
Burettes
Specimen
Filter papers
Cell pressure
Pore water pressure transducer
Heating/Cooling Circulator
Circulation pump
Pore pressure
PC

Figure 2

Click here to access/download;Figure;Figure 2.tif

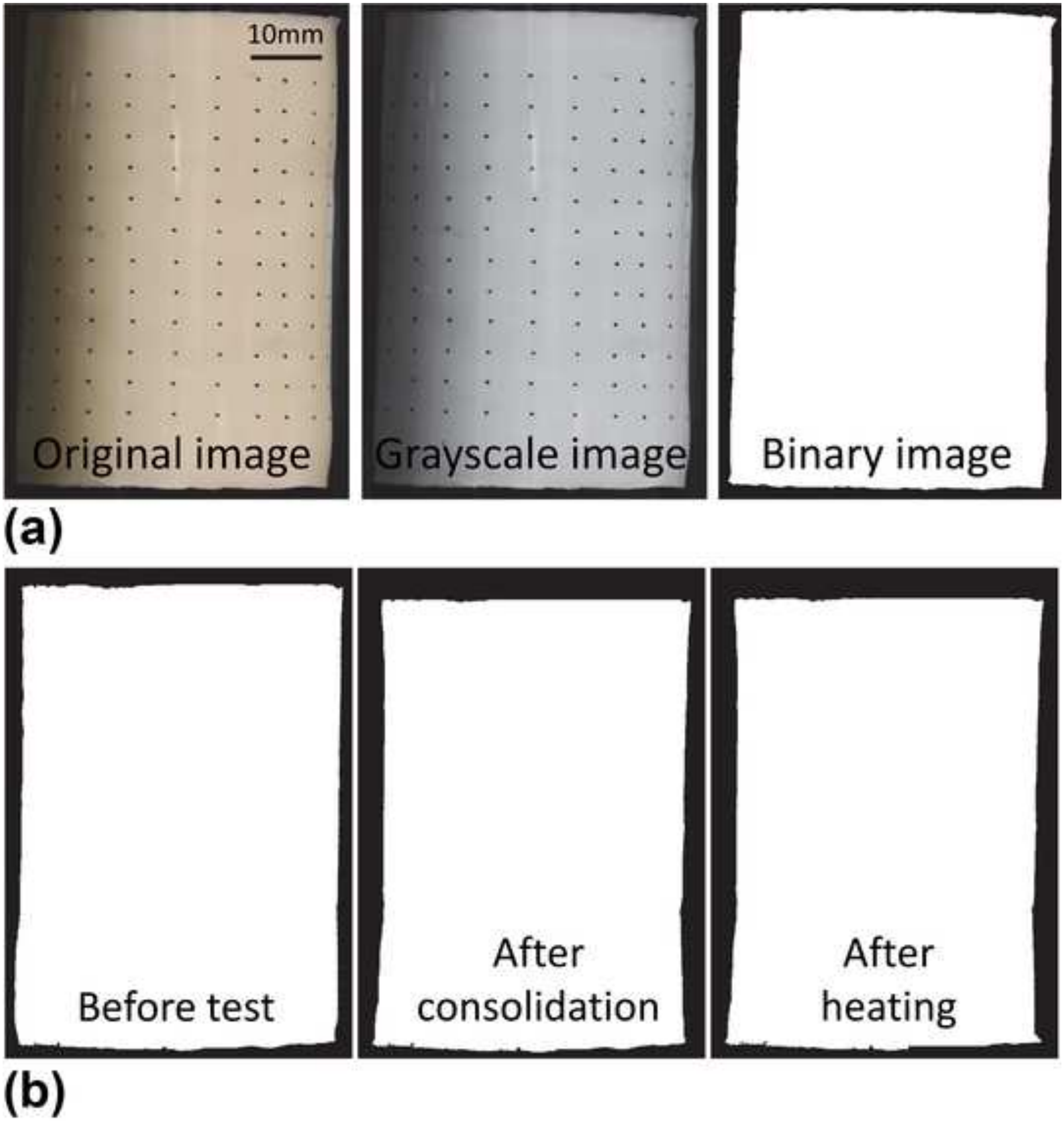

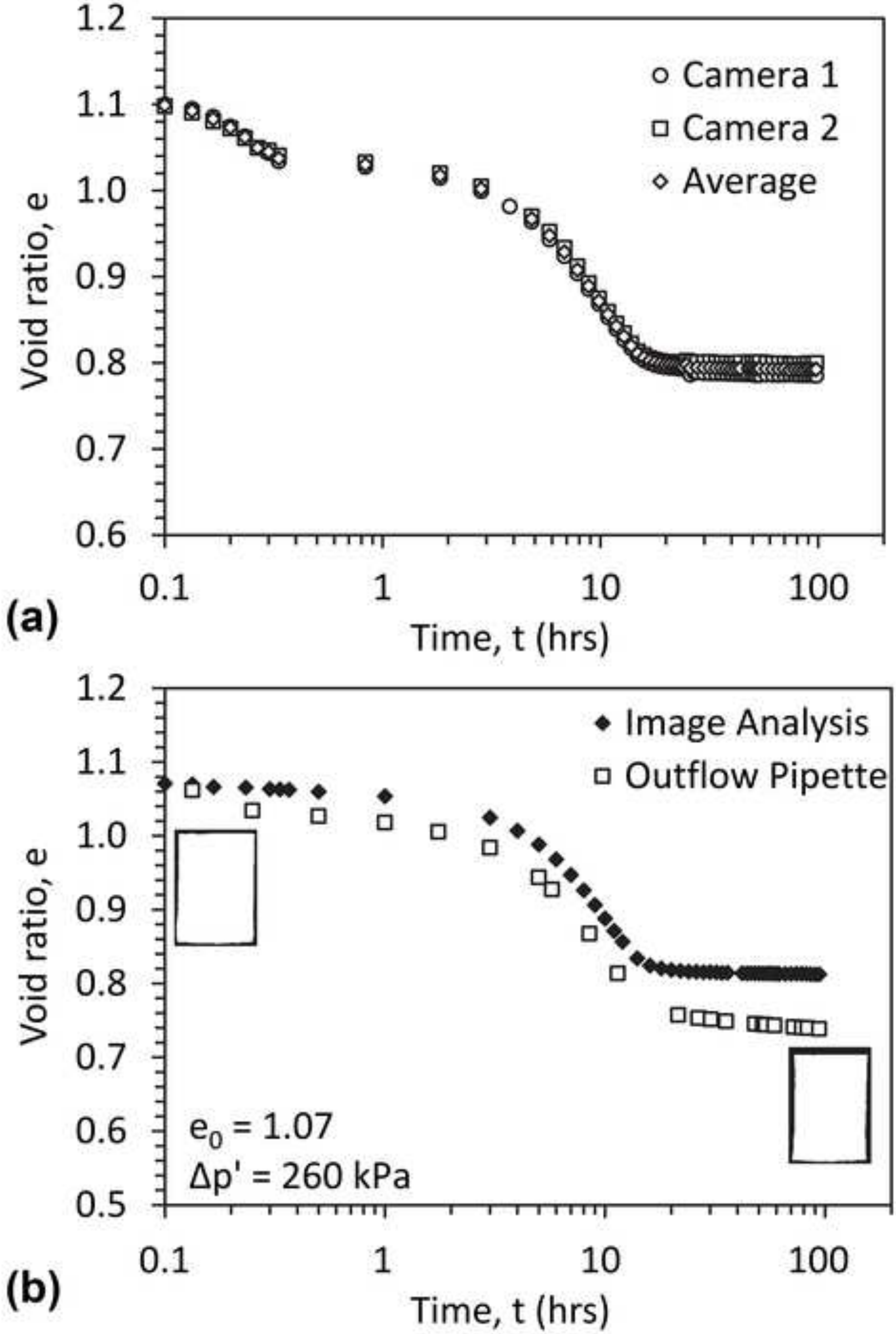
Void ratio, e
Camera 1
Camera 2
Average
1.2
1.1
1.0
0.9
0.8
0.7
0.6
0.1
1
10
100
(a)
Time, t (hrs)
Image Analysis
Outflow Pipette
0.5
e0 = 1.07
Δp' = 260 kPa
(b)

Figure 4

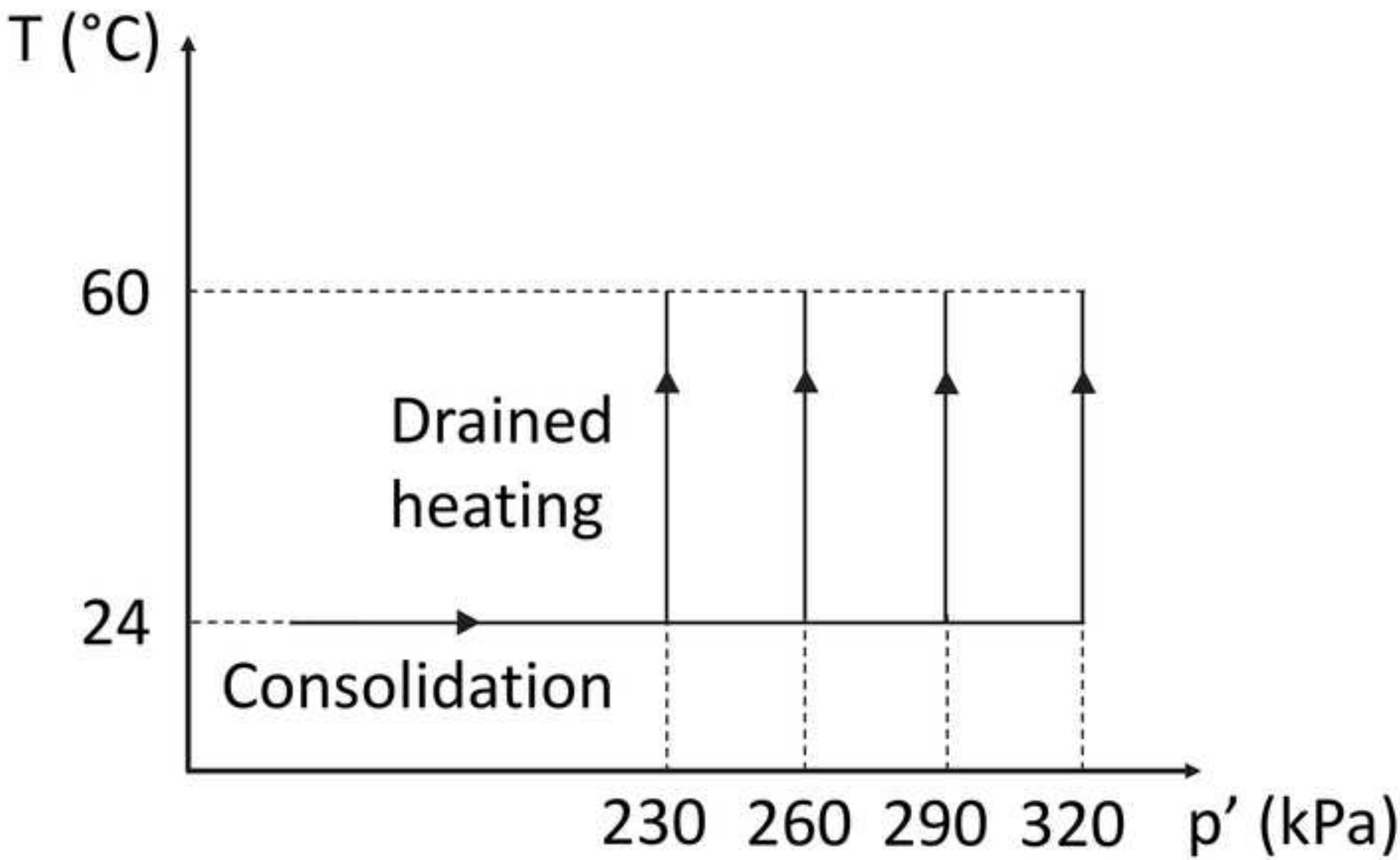

Figure 5

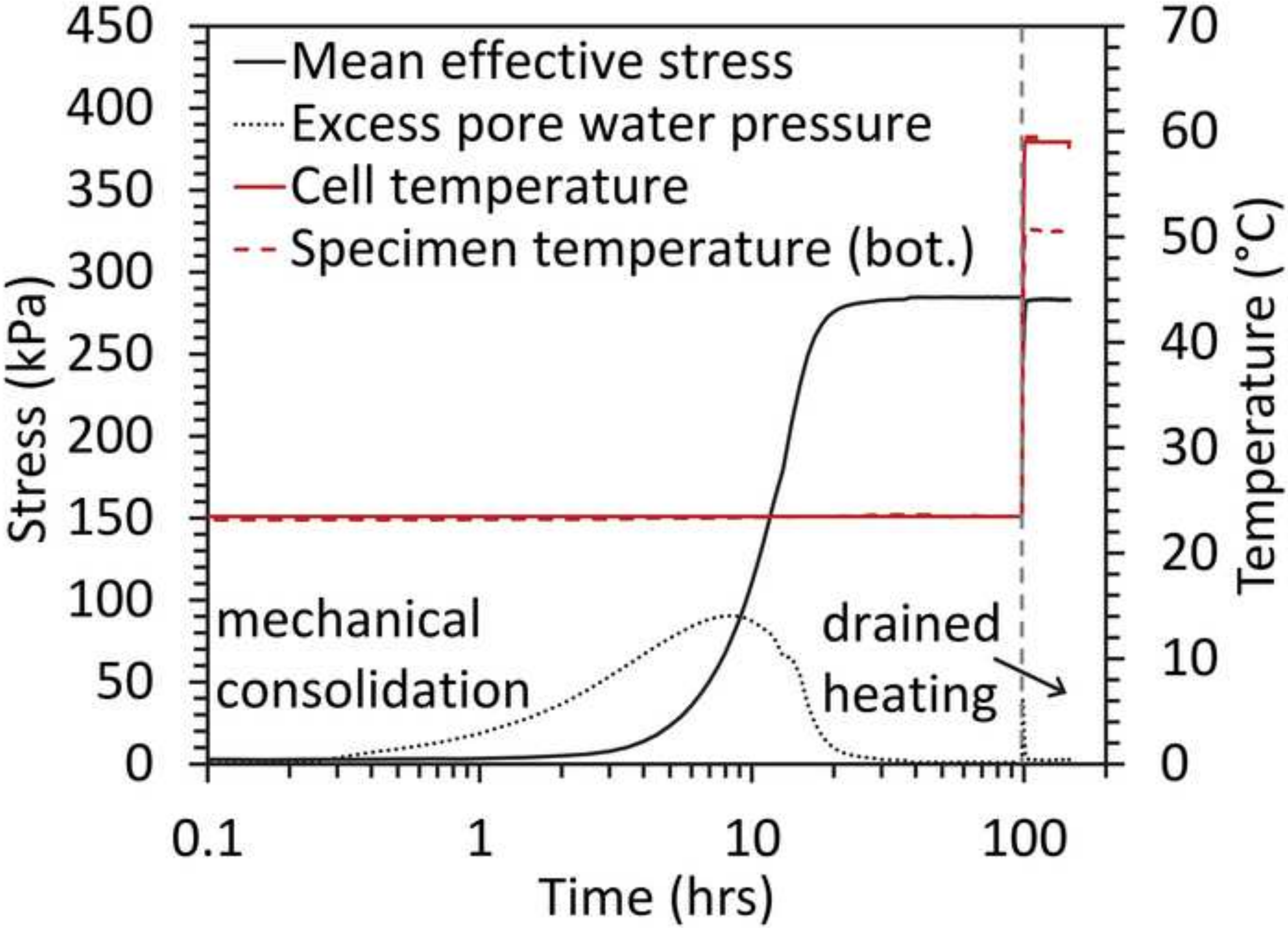

450
400
350
300
250
200
150
100
50
0
Stress (kPa)
70
60
50
40
30
20
10
0
Temperature (°C)
Mean effective stress
Excess pore water pressure
Cell temperature
Specimen temperature (bot.)
mechanical
consolidation
drained
heating
0.1
1
10
100
Time (hrs)

Figure 6

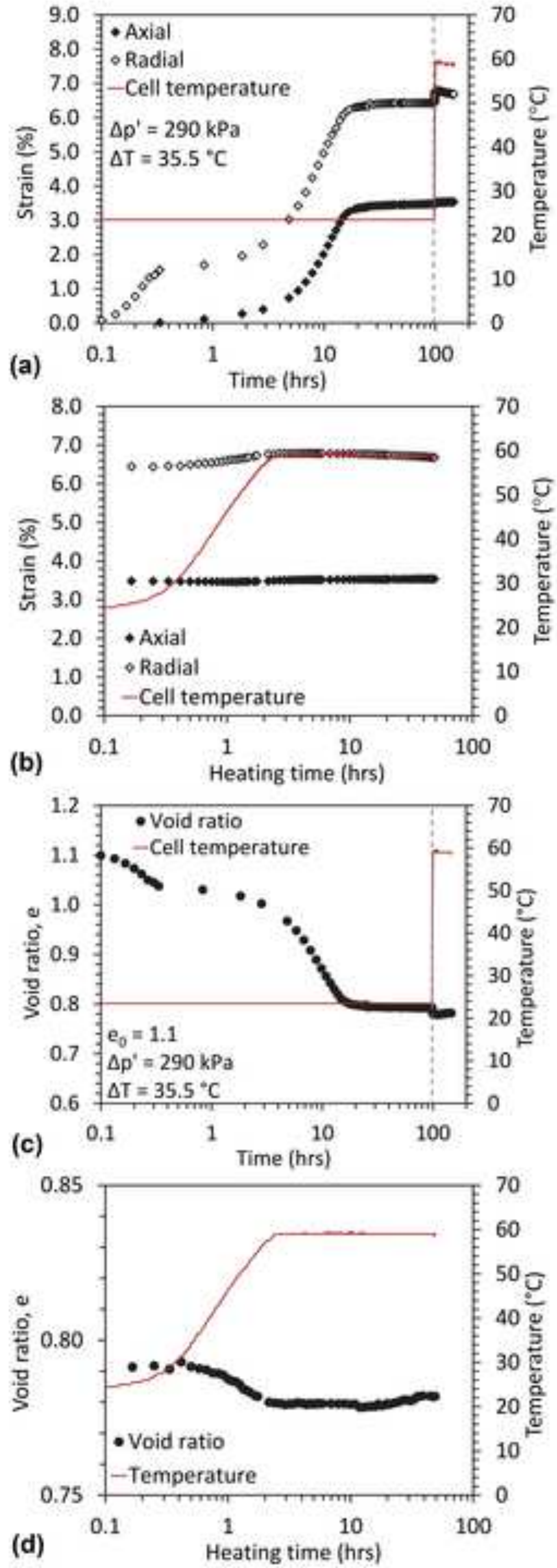

Axial
Radial
Cell temperature
Δp' = 290 kPa
ΔT = 35.5 °C
Strain (%)
Temperature (°C)
Time (hrs)
(a)
Heating time (hrs)
(b)
Void ratio
e0 = 1.1
Void ratio, e
(c)
Temperature
(d)

Figure 7

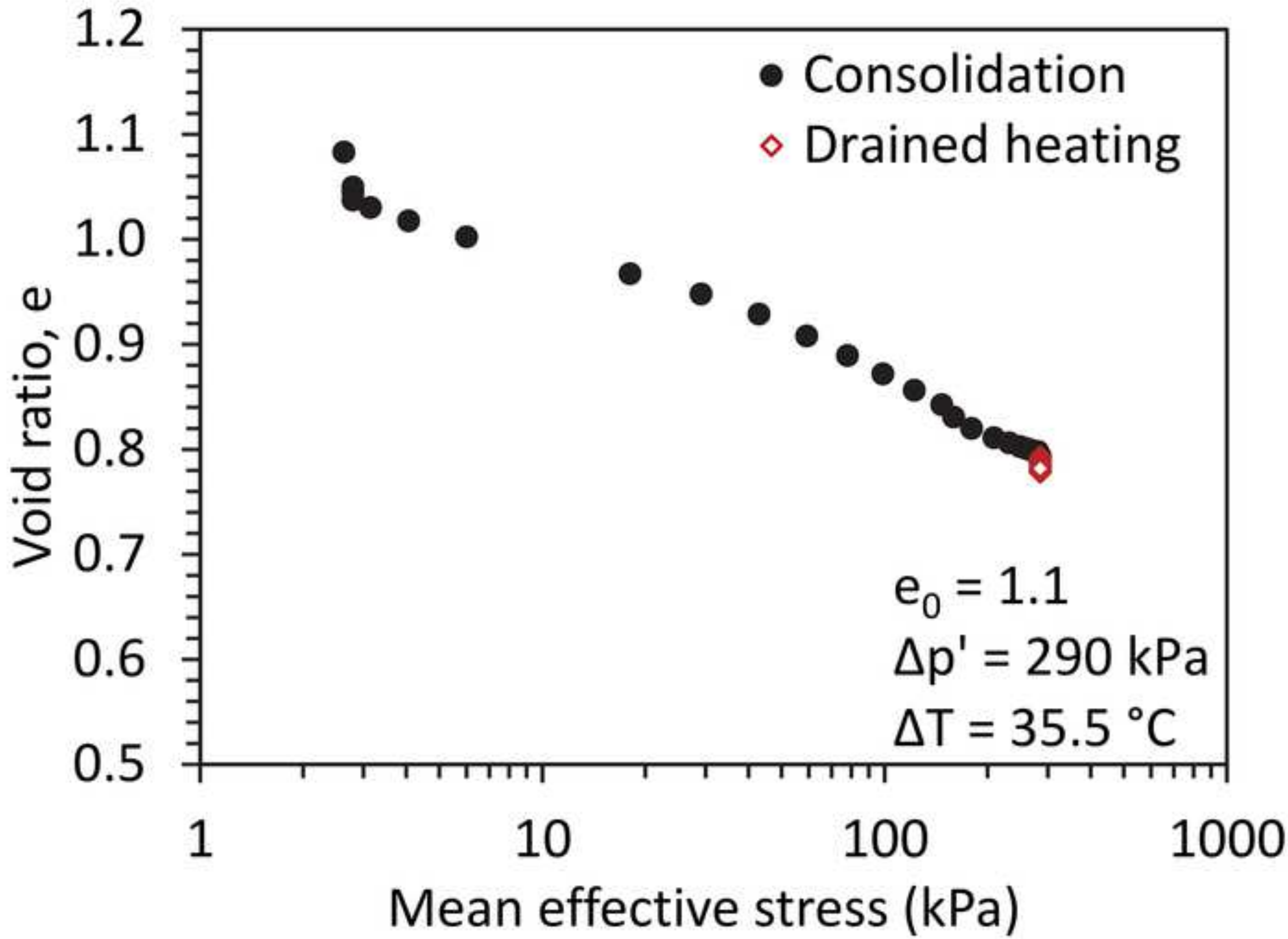

1.2
1.1
1.0
0.9
0.8
0.7
0.6
0.5
Void ratio, e
Consolidation
Drained heating
e0 = 1.1
Δp' = 290 kPa
ΔT = 35.5 °C
1
10
100
1000
Mean effective stress (kPa)

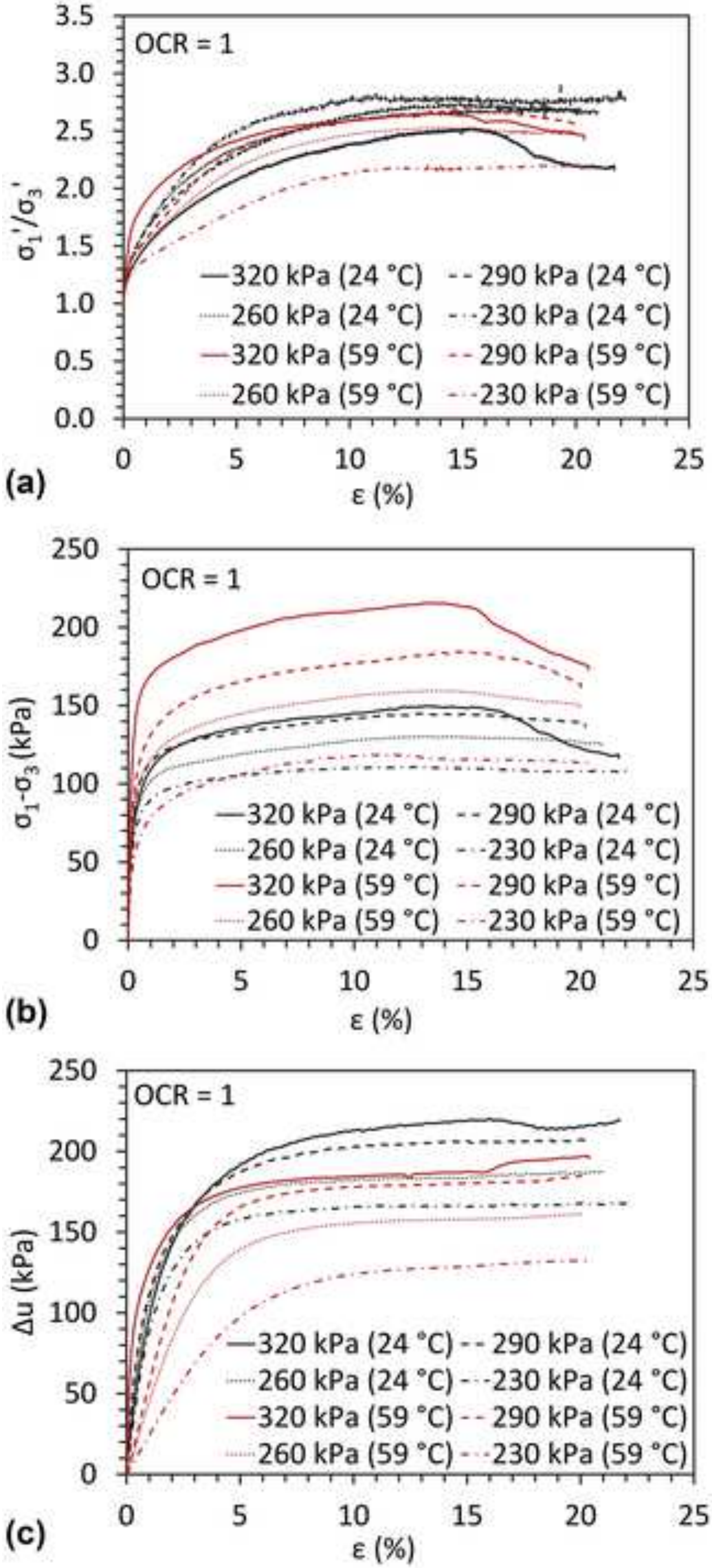
OCR = 1
σ1'/σ3'
ε (%)
(a)
320 kPa (24 °C)
290 kPa (24 °C)
260 kPa (24 °C)
230 kPa (24 °C)
320 kPa (59 °C)
290 kPa (59 °C)
260 kPa (59 °C)
230 kPa (59 °C)
OCR = 1
σ1-σ3 (kPa)
ε (%)
(b)
OCR = 1
Δu (kPa)
ε (%)
(c)

Figure 9

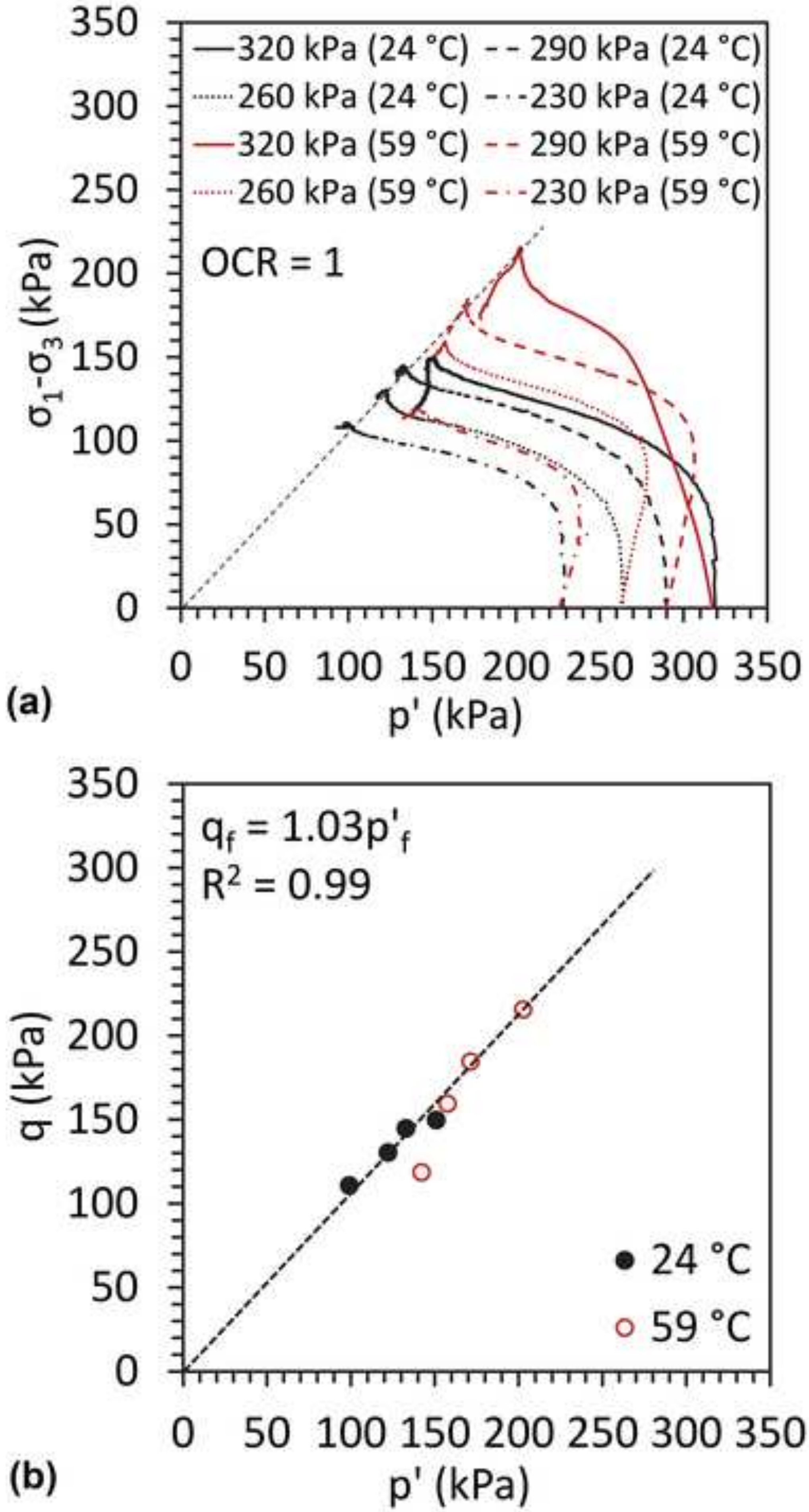

320 kPa (24 °C)
290 kPa (24 °C)
260 kPa (24 °C)
230 kPa (24 °C)
320 kPa (59 °C)
290 kPa (59 °C)
260 kPa (59 °C)
230 kPa (59 °C)
OCR = 1
σ_1-σ_3 (kPa)
p' (kPa)
(a)
$q_f = 1.03p'_f$
$R^2 = 0.99$
24 °C
59 °C
q (kPa)
p' (kPa)
(b)

Figure 10

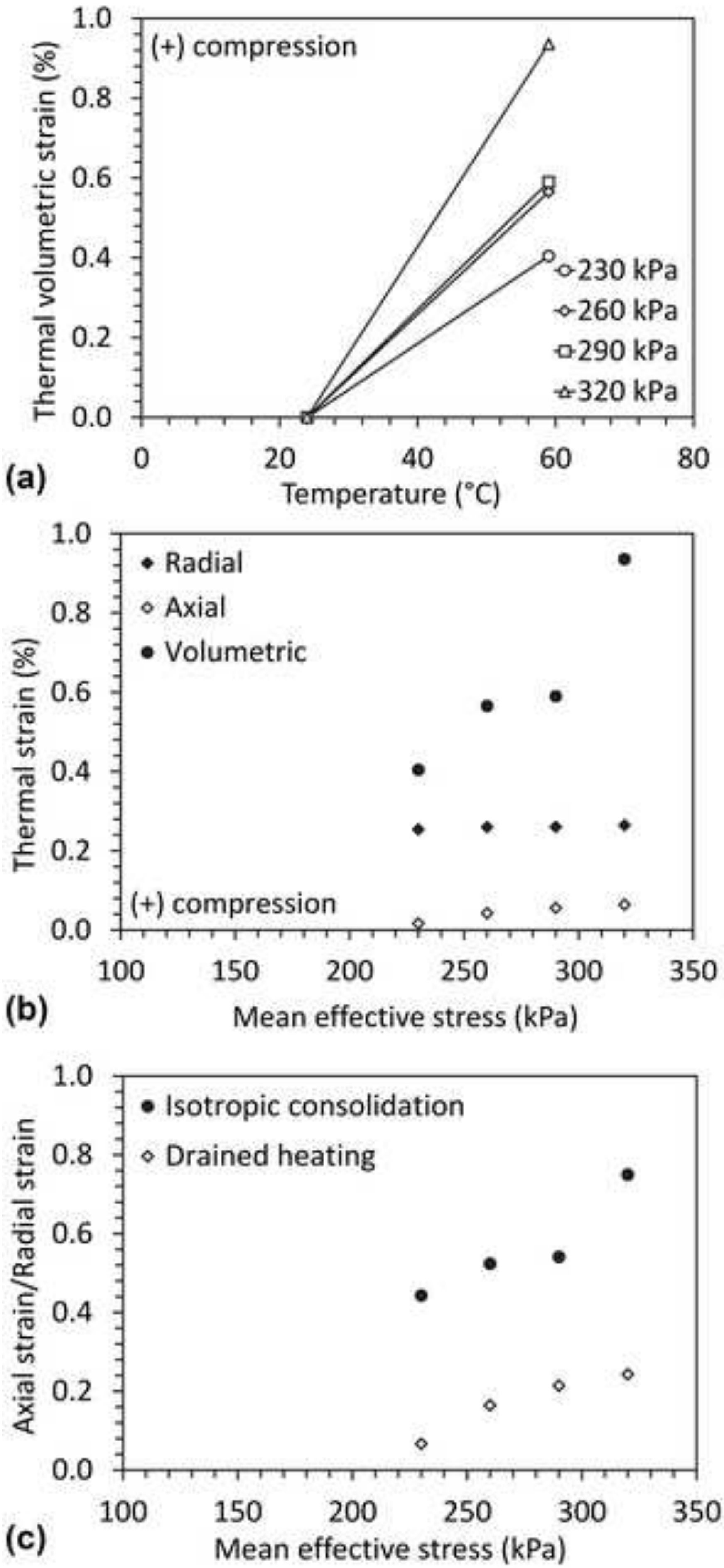

1.0
0.8
0.6
0.4
0.2
0.0
Thermal volumetric strain (%)
(+) compression
230 kPa
260 kPa
290 kPa
320 kPa
0
20
40
60
80
Temperature (°C)
(a)
1.0
0.8
0.6
0.4
0.2
0.0
Thermal strain (%)
Radial
Axial
Volumetric
(+) compression
100
150
200
250
300
350
Mean effective stress (kPa)
(b)
1.0
0.8
0.6
0.4
0.2
0.0
Axial strain/Radial strain
Isotropic consolidation
Drained heating
100
150
200
250
300
350
Mean effective stress (kPa)
(c)

Figure 11

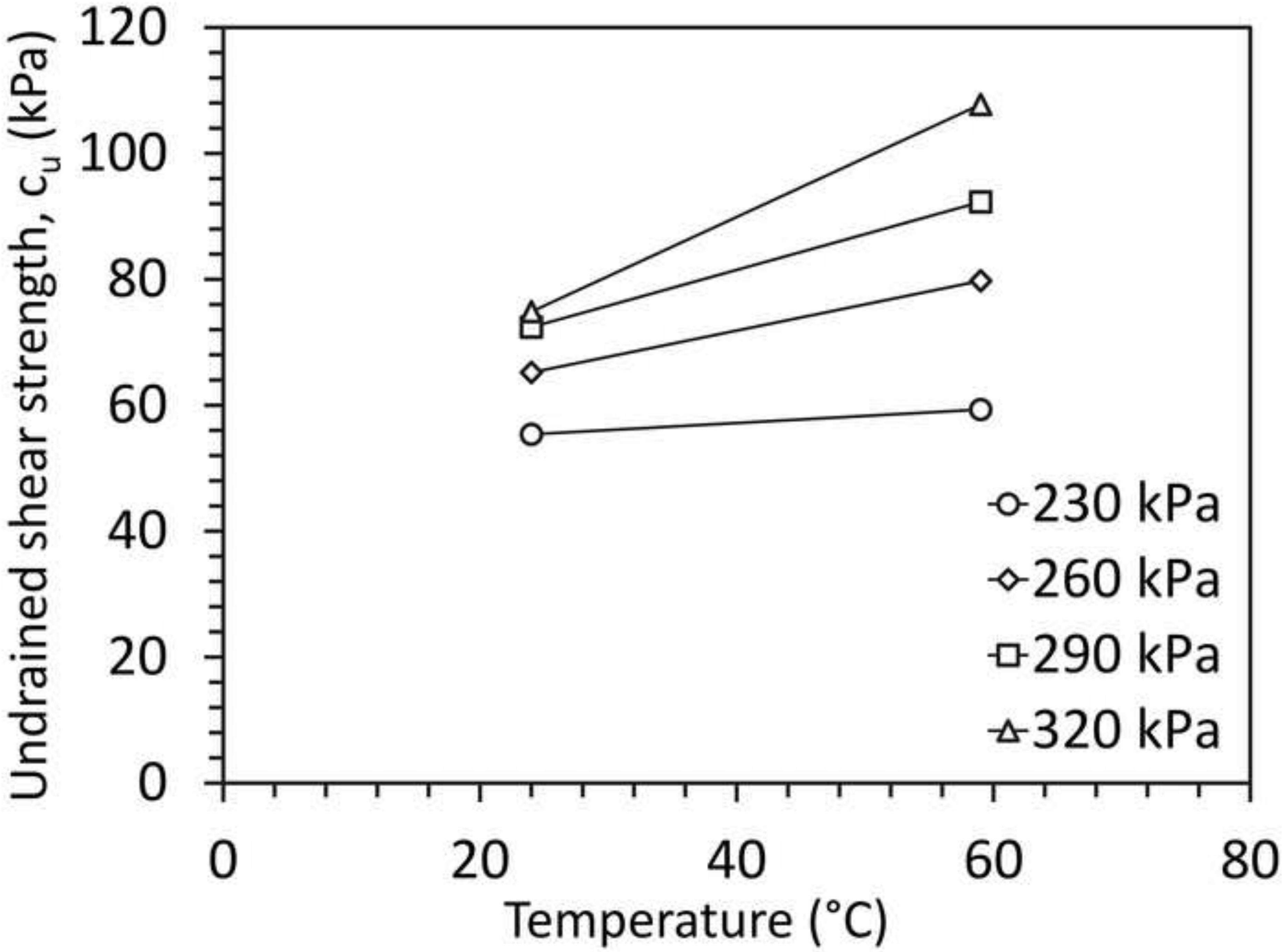
Undrained shear strength, c_u (kPa)
120
100
80
60
40
20
0
0
20
40
60
80
Temperature (°C)
230 kPa
260 kPa
290 kPa
320 kPa

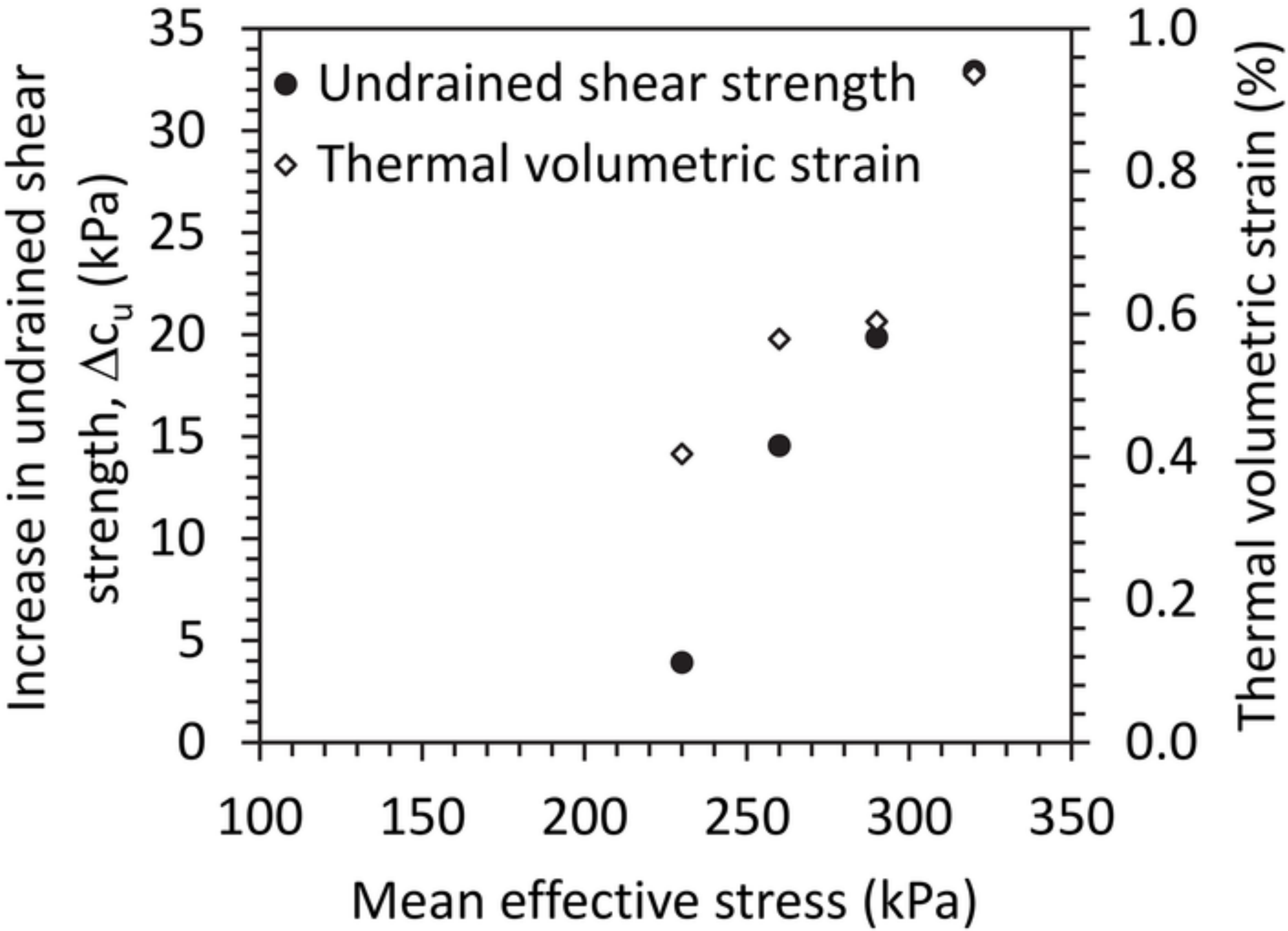

Undrained shear strength
Thermal volumetric strain
Increase in undrained shear strength, Δc_u (kPa)
Thermal volumetric strain (%)
Mean effective stress (kPa)
35
30
25
20
15
10
5
0
1.0
0.8
0.6
0.4
0.2
0.0
100
150
200
250
300
350